Appl. Phys. B 85, 173–180 (2006)
DOI: 10.1007/s00340-006-2362-3

Applied Physics B
Lasers and Optics

A.K.Y. NGAI✉
S.T. PERSIJN
G. VON BASUM
F.J.M. HARREN

Automatically tunable continuous-wave optical parametric oscillator for high-resolution spectroscopy and sensitive trace-gas detection

Life Science Trace Gas Facility, Molecular and Laser Physics, Institute for Molecules and Materials, Radboud University, 6525 ED Nijmegen, The Netherlands

Received: 18 May 2006/Revised version: 12 June 2006
Published online: 18 July 2006 • © Springer-Verlag 2006

ABSTRACT We present a high-power (2.75 W), broadly tunable (2.75–3.83 μm) continuous-wave optical parametric oscillator based on MgO-doped periodically poled lithium niobate. Automated tuning of the pump laser, etalon and crystal temperature results in a continuous wavelength coverage up to 450 cm^{-1} per poling period at $< 5 \times 10^{-4}$ cm^{-1} resolution. The versatility of the optical parametric oscillator as a coherent light source in trace-gas detection is demonstrated with photoacoustic and cavity ring-down spectroscopy. A 17-cm^{-1}-wide CO_2 spectrum at 2.8 μm and multi-component gas mixtures of methane, ethane and water in human breath were measured using photoacoustics. Methane (at 3.2 μm) and ethane (at 3.3 μm) were detected using cavity ring-down spectroscopy with detection limits of 0.16 and 0.07 parts per billion by volume, respectively. A recording of $^{12}CH_4$ and $^{13}CH_4$ isotopes of methane shows the ability to detect both species simultaneously at similar sensitivities.

PACS 42.65.Yj; 42.72.Ai; 42.62.Fi

1 Introduction

The detection of trace gases plays an important role in atmospheric and life science research. For instance, to have a proper understanding of global warming, it is important to understand the processes that govern the climate system [1]. Two very important greenhouse gases that are influenced by anthropogenic activities are carbon dioxide and methane. Only recently, Keppler et al. reported to have found that plants are responsible for significant methane emissions [2]. Although highly sensitive detection methods are necessary to determine the minute quantities of methane that are produced by an individual plant, the total contribution of plants can have important implications for the global methane budget. Also, in life science carbon dioxide and methane are indicators of all kinds of processes. For example, the respiration of insects can be monitored by detecting carbon dioxide trace emissions [3] and methane has been detected to study the behavior of plants [4], insects [5] and humans [6].

Trace-gas detectors based on laser spectroscopy are ideal instruments for detecting low quantities of multiple gases with high species selectivity. For this, challenging properties are needed in the form of novel coherent mid-infrared sources and detection methods. The envisioned high sensitivity for trace-gas species requires low-noise light sources with high power (watt level). A high spectral selectivity for molecular gases and the total-profiling capability require a maximum coverage of the molecular fingerprint region (2–20 μm), with sufficient spectral resolution (< 100 MHz). In addition, for a fast detection time response such novel mid-infrared sources have to provide superior wavelength agility. Such demanding properties can be met using continuous-wave optical parametric oscillators (cw OPOs) [7–12] in combination with sensitive spectroscopic techniques like photoacoustic spectroscopy [13–17] or cavity ring-down spectroscopy [18–21].

Photoacoustic spectroscopy is a technique whose sensitivity lies in a proper, adapted design of the photoacoustic gas cell to the coherent light source. The sensitivity scales with power, so to be able to detect sub-ppbv (parts per billion by volume, $1 : 10^9$) concentrations a high-power (watt-level) coherent light source is necessary, such as a continuous-wave optical parametric oscillator. Continuous-wave OPO photoacoustic spectroscopy gives a sensitive trace gas detection method with a very large dynamic range (10^8) and easy alignment.

With continuous-wave cavity ring-down spectroscopy (cw CRDS) similar trace-gas sensitivities can be reached. It has two advantages over photoacoustic spectroscopy. Firstly, this technique directly detects the absorption strength, while photoacoustic spectroscopy produces an acoustic signal that is linked to absorption. Secondly, the method is independent of light power, which makes it very useful in combination with low-power lasers. However, the sensitivity of CRDS depends on the high reflectivity of the cavity mirrors, which is a disadvantage. Mirrors are required with a very high reflectivity (> 99.98%) that can only be maintained over shorter-wavelength regions of approximately 100 nm (in the mid infrared). Also, the high finesse of the cavity requires good mode matching and thus very precise alignment of the cavity to the coherent source. Finally, the dynamic range of cavity ring-down spectroscopy is limited by the long effective path length in the cavity of several kilometers. For gases with strong absorptions in the mid-infrared region, such as methane, a typical maximum concentration of 100 ppbv can be reached when measuring a single absorption feature (for

✉ Fax: +31-(0)-24-365-33-11, E-mail: a.ngai@science.ru.nl

photoacoustic spectroscopy typically 1000 ppmv). The dynamic range of both methods could be extended by monitoring a spectral window containing absorption lines of different strengths. However, this sometimes requires scans over wider wavelength ranges.

Here we report on a continuous-wave, singly resonant, optical parametric oscillator in combination with both photoacoustic spectroscopy and cavity ring-down spectroscopy. In contrast to our former cw OPO setups [3], a periodically poled lithium niobate crystal with MgO doping (PP-MgO-LN) has been utilized, resulting in a substantial increase in power stability. While a change in wavelength of 1 cm^{-1} could require realignment of the entire cavity in the previous setup, the OPO now gives steady output power on the order of 1 W for the entire wavelength range. This has made automatic scanning of the OPO over large wavelength ranges at high resolution feasible. In the past, high-resolution scans (< 300 MHz) have been reported by various groups over limited wavelength ranges [10, 11, 20]. Also, broadly tunable (10 cm^{-1}) OPOs have been reported before using the translation of a fan-out periodically poled lithium niobate (PPLN) crystal in combination with a rotating etalon [14]. However, translation of the PPLN crystal can affect the OPO performance, because in time bad spots (local damage) occur in almost all PPLN crystals. Continuous-wave OPOs that are able to scan over hundreds of GHz at a resolution $< 5 \times 10^{-4}$ cm^{-1} have not been reported yet. Here we have demonstrated such wide, high-resolution scans by applying a combination of tuning techniques in a high-power OPO, based on PP-MgO-LN. The versatility and sensitivity of this system for trace-gas detection of several species and multiple-component gas mixtures has been shown with photoacoustic and cavity ring-down spectroscopy.

2 Experimental setup

The singly resonant OPO cavity consists of a standard four-mirror bowtie ring design (Fig. 1) [11, 22]. An MgO-doped periodically poled lithium niobate (PP-MgO-LN) crystal is placed between two concave mirrors ($R =$ 10 cm). The remaining two mirrors are flat. All mirrors are highly transparent for pump and idler, and highly reflective for the signal wavelength ($\geq 99.8\%$ R at 1350–1500 nm). The OPO is pumped by a single-frequency master oscillator–power amplifier system (Lightwave M6000), which generated as much as 11.5 W at 1064 nm and could be continuously tuned over 48 GHz. This laser combines a narrow line width (5 kHz over 1 ms) with a high frequency stability (50 MHz/h) and an excellent beam quality of $M^2 < 1.1$ in a TEM_{00} spatial mode. A half-wave plate (HWP) and a polarizing beam splitter (PBS) were placed after the pump laser so as to be able to control the pump power without causing any thermal disturbances in the laser.

In contrast to previous experiments, an MgO-doped (5 mol %) congruent PPLN crystal ($50 \times 8.4 \times 0.5$ mm) with poling periods ranging from 29.0 to 31.5 μm (HC Photonics) was used. Doping with MgO renders several advantages, such as a three orders of magnitude higher damage threshold and a wide operating temperature range [23]. The reason for this is a higher photoconductivity which reduces the photorefractive damage of the crystal, and a reduction of green-induced infrared absorption [24]. The power stability during temperature tuning of PP-MgO-LN is much better as compared to undoped material, where the OPO often ceased operation.

To control the cavity modes of the OPO, an uncoated 400-μm-thick solid YAG etalon (free spectral range 207 GHz) was mounted on a galvo driver inside the OPO cavity. With

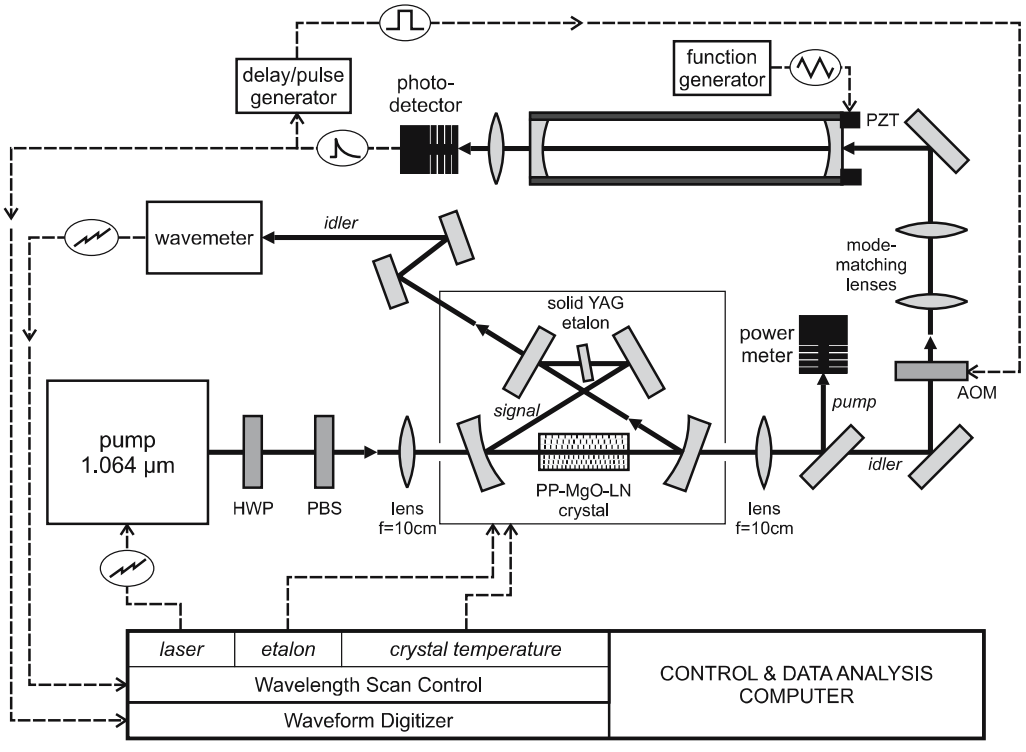

FIGURE 1 Experimental setup of the cw singly resonant OPO combined with continuous-wave cavity ring-down spectroscopy. The OPO cavity is resonant for the signal wavelength. The idler beam is sent to a cw ring-down cavity and to a wavemeter (HWP: half-wave plate, PBS: polarizing beam splitter, PP-MgO-LN: MgO-doped periodically poled lithium niobate)

the etalon and without any form of active stabilization, we observed a frequency stability of 4.5 MHz over 1 s by averaging the mode spectrum of a high-finesse cavity and 200 MHz over 300 s. Since the wavelength is continuously monitored at high resolution via a wavemeter, only the short-term drift over 1 s is important for the recorded spectra. A line width of 7 kHz over 20 μs was observed, which was determined by analyzing the monochromatic light in the scanning high-finesse ring-down cavity (free spectral range = 253 MHz, finesse = 18 500, line width = 14 kHz) following Müller et al. [25]. The idler and signal frequencies can be tuned between 2.75–3.83 μm and 1.47–1.73 μm, respectively, as were measured using a Burleigh WA-1000 wavemeter and an Advantest Q8382 optical spectrum analyzer. The tuning range was limited by the mirror coatings of the cavity for the signal [26]. The maximum idler output power of the OPO is 2.75 W.

For the trace-gas experiments we used a photoacoustic cell similar to the one described by van Herpen et al. [3]. The acoustic resonator has an inner radius of 2 mm and a length of 300 mm. The idler beam of the OPO was amplitude modulated at 560 Hz, exciting the lowest longitudinal mode of the acoustic resonator [27]. Three electret microphones (Knowless EK3024) mounted at the center of the acoustic resonator were used to detect the acoustic signal. The resonant acoustic enhancement combined with narrow-bandwidth lock-in detection enables ultra-sensitive detection at sub-ppbv levels.

The setup for cw CRDS (Fig. 1) consists of a germanium acousto-optic modulator (AOM, 100 MHz), a ring-down cavity ($L = 59.4$ cm) and a fast (HgCdZn)Te photodetector (VIGO System PDI2-TE4). The AOM deflects a part of the idler beam (20%) under an angle of 15 degrees towards the ring-down cavity. The ring-down cavity itself is a high-finesse optical resonator formed by two mirrors with a high-reflective coating around 3.3 μm ($R = 99.98\%$, Los Gatos Research). The length of the cavity was swept continuously at a rate of 30 Hz over one free spectral range by means of a piezoelectric transducer (PZT) to bring the cavity into resonance with the laser wavelength. As soon as the build up of intensity in the cavity reached a predetermined threshold, the AOM was switched off. The exponential decay of the intracavity radiation on the detector was then recorded using a waveform digitizer (Gage Compuscope CS14100) and fitted using a fast exponential fitting algorithm by Halmer et al. [28]. A pressure- and flow-control system was used to keep the pressure in the ring-down cavity at 100 mbar and supply the gas mixtures.

3 OPO wavelength tuning

The advantage of a singly resonant OPO lies in its ease of use for performing wavelength scans. If the pump laser wavelength is scanned, the OPO acts as a passive wavelength converter; by keeping the signal frequency fixed, the idler will follow the pump wavelength. Here, we used a Lightwave M6000 MOPA. This is a high-power pump source with a wide continuous tuning range and a narrow line width. We tuned the pump laser OPO combination in three stages:

Firstly, we scanned the pump laser continuously over 48 GHz. Hence, the idler wavelength will be tuned with the same frequency stability and line width as the pump laser, keeping the signal wavelength fixed within the OPO cavity. Although mode hops occur every 12 GHz in the idler due to mode hops in the pump laser, all wavelengths are still covered

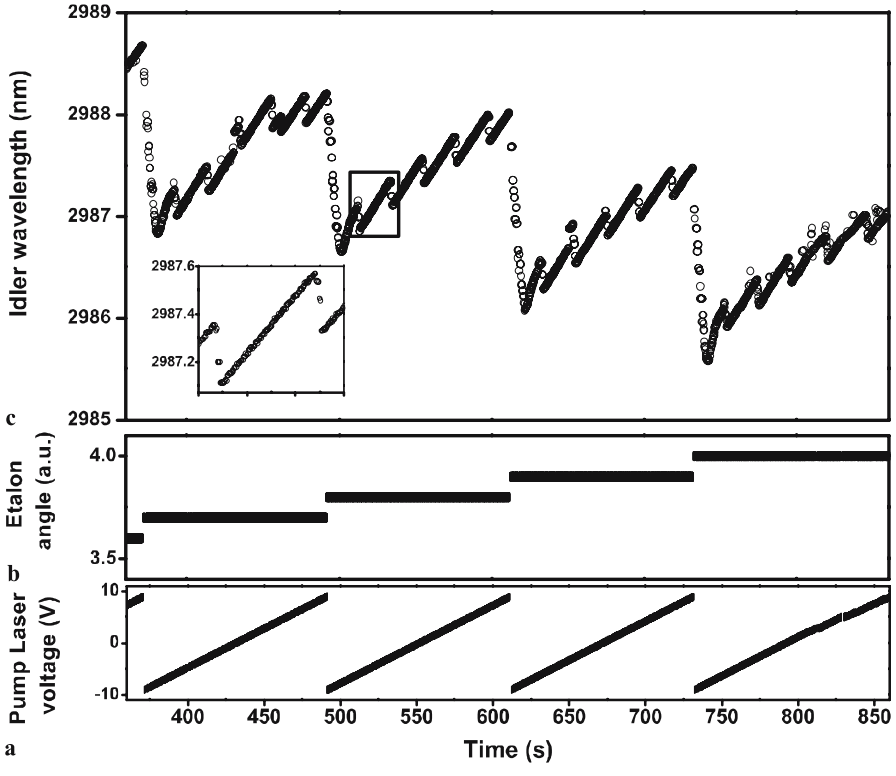

FIGURE 2 Combined pump–etalon scan. By scanning the pump laser (**a**) and stepping the etalon angle after each pump laser scan (**b**), a continuous wavelength coverage over 207 GHz can be realized (**c**). The resolution of the idler frequency is limited by the resolution of the wavemeter (*inset* in (**c**))

(Fig. 2). Secondly, a 207-GHz idler tuning can be achieved by tilting the intracavity etalon in the OPO. Discrete steps in the idler frequency occurred of the order of 0.07 cm^{-1} due to cluster hopping over the cavity mode spacing of 0.01 cm^{-1} [26, 29]. Thirdly, by changing the crystal temperature by 1 °C, 1–4 cm^{-1} of idler tuning is achieved, depending on the crystal period and the temperature. Temperature tuning of the OPO cavity without an intracavity etalon results in discrete steps in the idler frequency in the order of 0.3–1.5 cm^{-1}.

These three scanning methods were combined to cover an extended wavelength range with high resolution. At a fixed etalon angle the pump is scanned continuously (with mode hops every 12 GHz). Next, the etalon is tilted over a small angle and the pump is again scanned. This procedure is repeated until the free spectral range of the etalon (207 GHz) is covered. A combined pump-tuning etalon-stepping scan is shown in Fig. 2. After that, the crystal temperature is changed by 2–5 °C and the entire procedure is repeated. In this way, wavelength scans up to 450 cm^{-1} at a single period of the crystal are possible with high resolution ($< 5 \times 10^{-4}$ cm^{-1}). Although the same scan could be performed without varying the etalon angle, this process would be significantly slower due to the increased number of temperature changes. As compared to temperature tuning, varying the etalon angle also offers a more reproducible way of selecting a wavelength. The complete scanning process was fully automated and computer controlled, so that long wavelength scans and sensing of multiple gases over long periods of time was feasible.

By translating the PPLN crystal to other poling periods, access is provided to an idler wavelength range of 2.75 to 3.83 μm and a signal wavelength range of 1.47 to 1.73 μm. Figure 3 shows the signal and idler wavelengths as a function of the crystal temperature for six different grating periods. In addition, calculated values using the SNLO nonlinear optics software are shown [30]. The tuning curves for the different poling periods show a large overlap due to the wide crystal temperature range. In fact, this wavelength range could also be covered by using just three poling periods. A good consistency between calculated and measured wavelengths is obtained after uniformly shifting down the temperature axis 20 °C for the calculated wavelengths [14]. Partially, this can be explained by signal and idler absorption in the crystal. At an idler output power of 2 W at 3.4 μm the crystal temperature increased from room temperature to 50 °C, which is equal to 2.5 W of absorbed light power. This heating was not caused by pump beam absorption. Based on energy-conservation considerations, the temperature increase was mainly due to signal absorption. Although the signal absorption coefficient is lower, the intracavity signal power is much higher. To operate the OPO continuously at room temperature, the PP-MgO-LN crystal was water cooled, extending the operation temperature down to 18 °C.

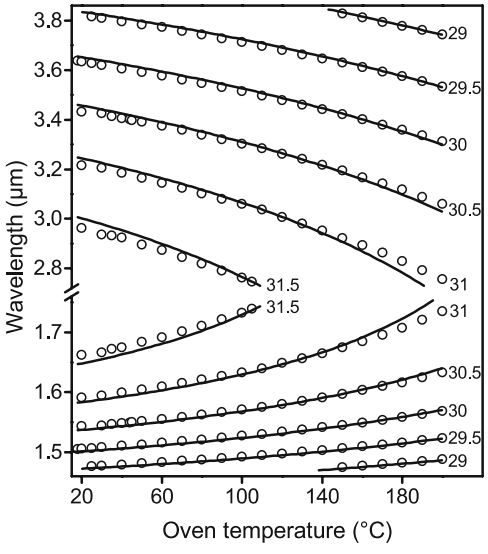

FIGURE 3 Signal (1475–1739 nm) and idler (2746–3829 nm) wavelengths of the OPO vs. temperature of the PP-MgO-LN crystal for poling periods 29.0–31.5 μm. The *solid lines* are the calculated values from SNLO

4 Detection of CO_2 by OPO photoacoustics at 2.8 μm

Figure 4a shows a photoacoustic recording of a part of the strong $10^0$1-000 and $02^0$1-000 combination bands of CO_2 at 1-bar pressure, demonstrating the capability of the OPO to cover a wide spectral range in the mid-infrared region. The water-vapor concentration in the flow was reduced by scrubbing the gas flow with $CaCl_2$ pellets. The contribution of each of the gases was determined by fitting the measured spectrum with the calculated spectra from the HITRAN database [31] (inset, Fig. 4a). The water-vapor spectrum was subtracted to reveal the CO_2 spectrum. In Fig. 4b a calculated CO_2 spectrum based on data from the HITRAN database is given. As can be seen, the photoacoustic spectrum is in excellent agreement with the calculations. The spectrum was recorded fully automatically by a combination of pump laser,

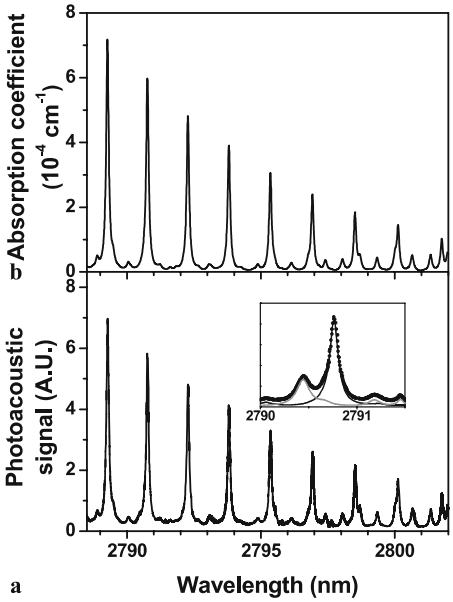

FIGURE 4 (**a**) Recorded photoacoustic spectrum of CO_2 in laboratory air (460 ppmv), corrected for the water-vapor contribution by subtracting the calculated water spectrum. The *inset* shows the calculated water-vapor (*gray line*) and CO_2 contributions (*black line*) of which the sum matches the recorded photoacoustic spectrum (*dots*). (**b**) CO_2 spectrum calculated from HITRAN

intracavity etalon and crystal temperature tuning. The resolution of the spectrum is 0.01 nm and was limited by the wavemeter, which was set to a lower resolution and a wider wavelength coverage. By monitoring the wavelength at each measured point, the complete spectrum can easily be constructed despite any mode hops or other jumps in wavelength that occurred. The recording time for the complete spectrum was approximately 1 h. This is mainly caused by spectral overlap in the different types of scan, so that it is guaranteed that no points are missed. By further optimizing the scanning method using the wavemeter for direct feedback, the scan time can be shortened considerably.

5 Photoacoustic detection of methane in human breath

The OPO is an ideal source for laser spectroscopy, because a spectral region can simply be chosen where the gas or multiple gases have strong absorptions with little or no interference from other gases, such as water vapor. We have demonstrated this by measuring the breath from two test persons at a wavelength range where there are absorptions from methane, ethane and water (Fig. 5b). Figure 5a depicts the calculated spectra from the HITRAN database for the three gases. The breath of both persons was collected first in bags (aluminum-coated Teflon). The bags were sampled by connecting them to a flow system with a flow rate of 5 l/h and a pressure in the photoacoustic cell of about 250 mbar. The concentrations of methane and ethane for test person 1 were determined to be 21 ppmv and 13 ppbv, respectively. The breath of test person 2 contained 4.5-ppmv methane, and 13-ppbv ethane. The reason for the increased concentration of methane in the breath of test person 1 can likely be explained by the presence of methanogenic flora in this person [32]. One of the strengths of photoacoustic spectroscopy is its wide dynamic range; only the lock-in sensitivity needs to be adjusted automatically during the scan. Although the concentrations for methane and ethane were three orders of magnitude apart from each other, they still could be measured simultaneously by selecting spectral areas where the difference in concentrations is partially compensated by the relative strengths of the absorption lines.

6 Detection of methane and ethane using OPO cavity ring-down spectroscopy

To determine the sensitivity of the OPO CRDS system, we measured methane (at 3.221 μm) and ethane (at 3.337 μm) for different concentrations in the ppbv range at 100-mbar pressure. Both absorption peaks were chosen based on calculated spectra from the HITRAN database. Conditions for this were high absorption strength and separated features from water, CO_2 and other atmospheric gases.

The methane mixtures were created by using different flows of N_2 (99.999% purity) and a certified mixture containing 90 ppbv methane buffered in N_2 (certified mixture, Air Liquide). For each concentration a scan was made over the absorption peak in a time lapse of 200 s with a spectral resolution of 0.001 cm^{-1}. The concentration was calculated by fitting the absorption peak and taking the area under the fitted curve. In this way all the measured points of the absorption profile are used, which leads to a higher sensitivity. The advantage of this method compared to a determination of a concentration on the top of an absorption peak is that any interference from other gases will be detected and can be taken into account. From the linear fit in Fig. 6 it can be seen that there is a relatively large background of 31-ppbv methane already present in the N_2 gas. The noise-equivalent detection limit for

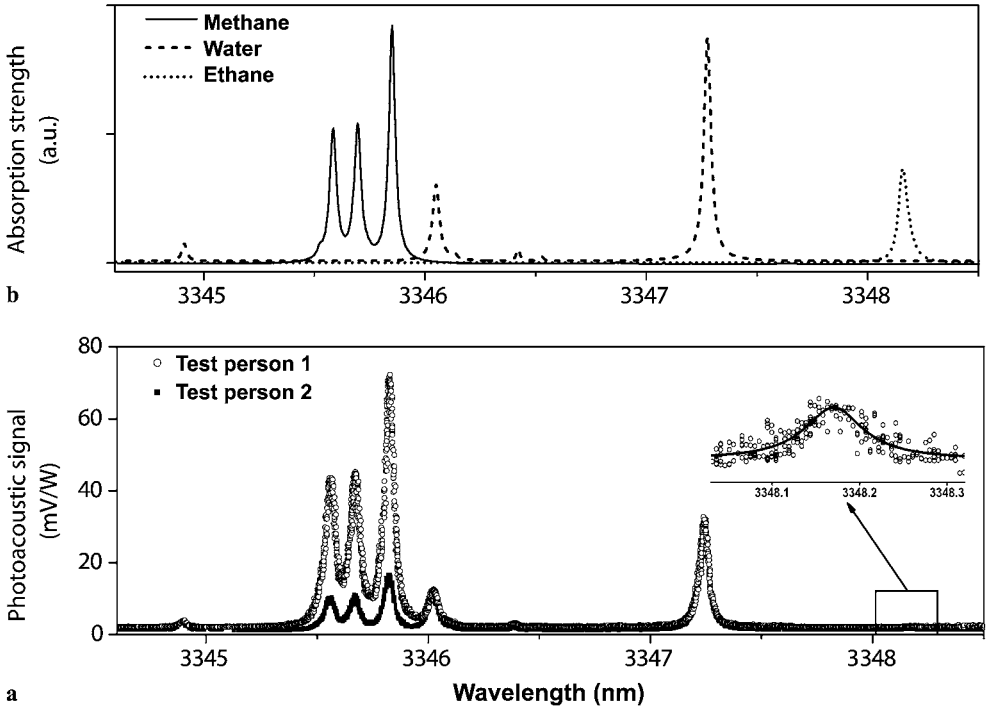

FIGURE 5 (**a**) Photoacoustic spectra measured from the breath of two different test persons. The recorded spectra reveal a higher methane concentration in the breath of person 1, indicating that methanogenic flora are present. (**b**) Calculated absorption spectra based on the HITRAN database for methane, ethane and water

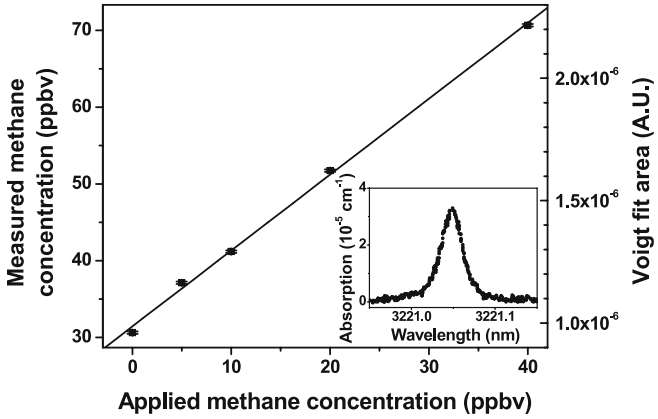

FIGURE 6 Areas of fitted methane absorption peaks for different concentrations. The wavelength of the OPO was scanned over the methane absorption feature (*inset*) in 200 s and measured with cavity ring-down spectroscopy. The linear fit reveals that a background methane concentration of 31 ppbv was present in the nitrogen. A noise-equivalent detection limit of 0.16 ppbv was found

methane using cw CRDS could be determined to be 0.16 ppbv over 200 s, corresponding to a minimum detectable absorption coefficient of 2.0×10^{-9} cm^{-1}. The larger errors at lower concentrations are partially caused by fluctuations in the methane flow during a scan. The background measurement given at 0 ppbv methane concentration uses only one flow directly from the nitrogen-gas bottle.

For the ethane mixtures, a certified mixture of 21 ppmv ethane buffered in nitrogen was used. The same scans were made over a shorter time period of 60 s and a lower wavemeter resolution of 0.01 cm^{-1}. The same procedure as for methane was followed for fitting and determining the concentrations. Figure 7 shows the different concentrations of ethane varying from 5 to 100 ppbv. A noise-equivalent detection limit of 0.07 ppbv over 60 s was determined from this graph, which corresponds to a minimum detectable absorption coefficient of 1.4×10^{-9} cm^{-1}.

Figure 8 shows a spectrum of $^{12}CH_4$ and $^{13}CH_4$ isotopes of methane in laboratory air recorded with continuous-wave cavity ring-down spectroscopy. The spectral region around 3.2 μm was chosen because of the relative strengths of the absorption peaks of $^{12}CH_4$ and $^{13}CH_4$. Since the abundance of $^{13}CH_4$ is a factor of 100 lower in the atmosphere than of $^{12}CH_4$, the ratio in absorption strengths for the two isotopes was chosen such that the absorption would be similar. This spectral region is also chosen for its low water-vapor interference. Because the absorption strengths of $^{13}CH_4$ are of the same order of magnitude as for $^{12}CH_4$, enriched mixtures of $^{13}CH_4$ can be detected with the same sensitivity.

One of the drawbacks of cavity ring-down spectroscopy is its limited spectral coverage. The sensitivity of the detection method depends on very high reflective mirrors, giving absorption path lengths of up to 3.5 km in our setup. The

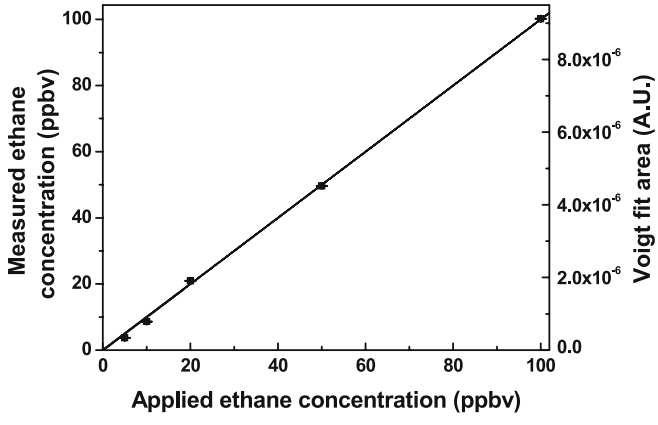

FIGURE 7 Areas of fitted ethane absorption peaks for different concentrations. The wavelength of the OPO was scanned over the ethane absorption feature in 60 s and measured with cavity ring-down spectroscopy. The noise-equivalent detection limit is 0.07 ppbv

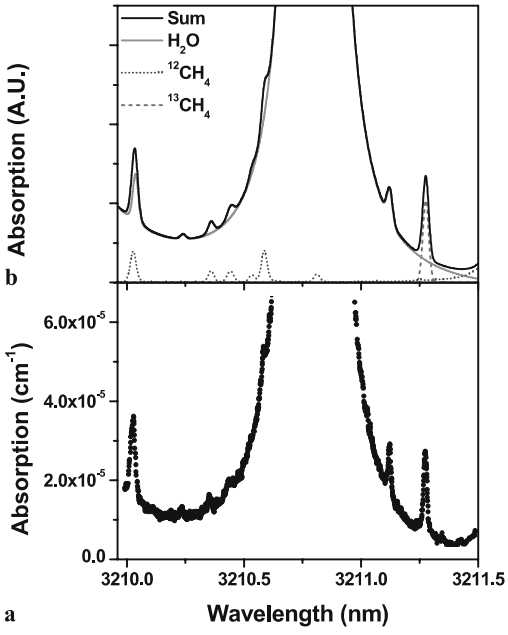

FIGURE 8 (**a**) Continuous-wave CRDS recording of the $^{12}CH_4$ and $^{13}CH_4$ isotopes in laboratory air. The natural abundance is partially compensated by selecting $^{12}CH_4$ peaks with two orders of magnitude weaker absorptions. (**b**) Calculated absorption spectra for H_2O, $^{12}CH_4$ and $^{13}CH_4$. The sum of the calculated absorption features shows a good correspondence to the measured data

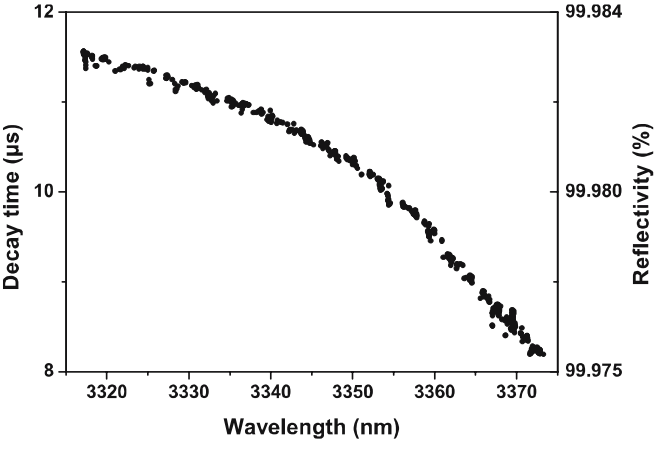

FIGURE 9 CRDS mirror reflectivity over 60-nm spectral range, demonstrating the limited wavelength range for each set of highly reflective mirrors. The drop in decay time from 11.6 to 8.2 μs gives an equivalent decrease in sensitivity

high reflectivity, however, can only be provided for wavelength ranges of typically 100 nm. Figure 9 shows a recording of the decay time and the cavity mirror reflectivity over 60 nm. The recording is a lower-resolution scan of the OPO by varying the crystal temperature only. Absorption peaks have been discarded, leaving only the maximum decay time at each wavelength given by the reflectivity of the cavity mirrors. It can be seen that a slight decrease in reflectivity will lead to much lower decay times and thus a lower sensitivity. In the measured wavelength range, the decay time dropped from 11.6 μs to 8.2 μs, corresponding to an equivalent decrease in sensitivity.

7 Discussion and conclusion

The versatility and sensitivity of a continuous-wave, singly resonant OPO combined with photoacoustic and cavity ring-down spectroscopy has been demonstrated as an instrument for trace-gas sensing. By using PP-MgO-LN instead of undoped PPLN, the OPO gained in power and wavelength stability. Moreover, the ability to operate the crystal from room temperature up to 200 °C resulted in a considerable increase of the crystal temperature tuning range. In the previous setup with an OPO based on conventional PPLN, the OPO could be observed to lose its power completely during larger wavelength changes by intracavity etalon or temperature tuning, thus requiring realignment of the OPO cavity. Additionally, the PPLN crystal had to be operated above 100 °C to counteract potential refractive damage.

Although the different tuning capabilities of pump, intracavity etalon and crystal temperature have already been recognized, automating all three methods has proven to be an effective way for recording wide, high-resolution spectra. It has been shown that a wide, continuous coverage can be achieved by using fan-out crystals as well [14, 33]. However, bad spots occur in the crystals with increasing age and if the crystals are used at these places, it often results in considerable damage to the crystal. Another advantage of stepped crystals with multiple poling periods is that a larger spectral range can be covered, since the difference in poling period lengths can have a greater variation. A typical fan-out crystal has poling periods between 29.3 and 30.1 μm, while our stepped crystal contains poling periods between 28.5 and 31.5 μm.

The spectral coverage of an OPO system also depends on the power of the pump source. Low oscillation thresholds can be achieved using longer PPLN crystals and higher mirror reflectivity, though the latter inherently leads to a narrowing of the spectral coverage. Double-resonant techniques to enhance the pump power in the OPO cavity can overcome threshold problems as well, but make tuning of the OPO complicated. Thanks to the high available pump power, idler wavelengths from 2.75 to 4.8 μm [3] have been reached, limited only by the intrinsic absorption of lithium niobate.

Photoacoustic spectroscopy is an ideal detection method for the OPO, taking full advantage of the high power and the wide spectral range available. Compared to cavity ring-down spectroscopy, alignment is simpler while similar trace gas detection sensitivities are reached. Photoacoustic spectroscopy, however, needs longer measuring times per data point (typically 100 ms), making it a slower spectroscopic method and thus prevents fast scanning. Higher repetition frequencies can be reached with cavity ring-down spectroscopy at low powers, such as what is available above 4 μm with our OPO [26].

CRDS with the OPO resulted in noise-equivalent detection limits of $2.0 \times 10^{-9}\,\mathrm{cm}^{-1}$ and $1.4 \times 10^{-9}\,\mathrm{cm}^{-1}$ for methane and ethane, respectively. These were lower than those found by von Basum et al. [6], which was mainly due to a lower decay rate and an etalon effect that could be observed from the cavity mirrors. The detection limit can be improved significantly by enabling the ring-down cavity for faster modulation frequencies and shortening the scan time by detecting at lower resolution. The approach of scanning over absorption features instead of measuring at the peak does give us the ability to distinguish between changes in concentration of the targeted species or the background caused by other absorption features.

A substantial advancement can be made in the scanning method of the OPO if it could offer continuous scanning capabilities without any excessive overlaps of mode hops and scans that occur at present. This development, which mainly lies in smarter tuning of the software, will result in cleaner spectra and shorter recording times. Combined with active stabilization of the OPO cavity, it would create an invaluable tool for high-resolution spectroscopy and the detection and identification of multiple, larger components in trace-gas detection.

ACKNOWLEDGEMENTS This research was financially supported by the Dutch Technologiestichting STW and the European Union under the program New and Emerging Science and Technologies, Contract No. FP6-NESTA-0025042 'Optical Nose'.

REFERENCES

1 J.T. Houghton and Intergovernmental Panel on Climate Change, Working Group I, *Climate Change 2001: the Scientific Basis: Contribution of Working Group I to the Third Assessment Report of the Intergovernmental Panel on Climate Change* (Cambridge University Press, New York, 2001)
2 F. Keppler, J.T.G. Hamilton, M. Brass, T. Rockmann, Nature **439**, 187 (2006)
3 M.M.J.W. van Herpen, A.K.Y. Ngai, S.E. Bisson, J.H.P. Hackstein, E.J. Woltering, F.J.M. Harren, Appl. Phys. B **82**, 665 (2006)
4 T.T. Groot, P.M. van Bodegom, F.J.M. Harren, H.A.J. Meijer, Biogeochemistry **64**, 355 (2003)
5 S.T. Persijn, E. Santosa, F.J.M. Harren, Appl. Phys. B **75**, 335 (2002)
6 G. von Basum, D. Halmer, P. Hering, M. Mürtz, S. Schiller, F. Müller, A. Popp, F. Kühnemann, Opt. Lett. **29**, 797 (2004)
7 W.R. Bosenberg, A. Drobshoff, J.I. Alexander, L.E. Myers, R.L. Byer, Opt. Lett. **21**, 1336 (1996)
8 P.E. Powers, T.J. Kulp, S.E. Bisson, Opt. Lett. **23**, 159 (1998)
9 M.E. Klein, C.K. Laue, D.H. Lee, K.J. Boller, R. Wallenstein, Opt. Lett. **25**, 490 (2000)
10 E.V. Kovalchuk, D. Dekorsy, A.I. Lvovsky, C. Braxmaier, J. Mlynek, A. Peters, S. Schiller, Opt. Lett. **26**, 1430 (2001)
11 M.M.J.W. van Herpen, S. te Lintel Hekkert, S.E. Bisson, F.J.M. Harren, Opt. Lett. **27**, 640 (2002)
12 I.D. Lindsay, B. Adhimoolam, P. Gross, M.E. Klein, K.J. Boller, Opt. Express **13**, 1234 (2005)
13 M.M.J.W. van Herpen, S.C. Li, S.E. Bisson, F.J.M. Harren, Appl. Phys. Lett. **81**, 1157 (2002)
14 S.E. Bisson, K.M. Armstrong, T.J. Kulp, M. Hartings, Appl. Opt. **40**, 6049 (2001)
15 F. Kühnemann, K. Schneider, A. Hecker, A.A.E. Martis, W. Urban, S. Schiller, J. Mlynek, Appl. Phys. B **66**, 741 (1998)
16 A.A. Kosterev, F.K. Tittel, D.V. Serebryakov, A.L. Malinovsky, I.V. Morozov, Rev. Sci. Instrum. **76**, 043 105 (2005)

17 M.W. Sigrist, Rev. Sci. Instrum. **74**, 486 (2003)
18 A. O'Keefe, D.A.G. Deacon, Rev. Sci. Instrum. **59**, 2544 (1988)
19 A. Popp, F. Müller, F. Kühnemann, S. Schiller, G. von Basum, H. Dahnke, P. Hering, M. Mürtz, Appl. Phys. B **75**, 751 (2002)
20 D. Halmer, G. von Basum, P. Hering, M. Mürtz, Opt. Lett. **30**, 2314 (2005)
21 Y.B. He, B.J. Orr, J. Chin. Chem. Soc. **48**, 591 (2001)
22 M.M.J.W. van Herpen, S. Li, S.E. Bisson, S. te Lintel Hekkert, F.J.M. Harren, Appl. Phys. B **75**, 329 (2002)
23 L. Arizmendi, Phys. Stat. Solidi A **201**, 253 (2004)
24 Y. Furukawa, K. Kitamura, A. Alexandrovski, R.K. Route, M.M. Fejer, G. Foulon, Appl. Phys. Lett. **78**, 1970 (2001)
25 F. Müller, G. von Basum, A. Popp, D. Halmer, P. Hering, M. Mürtz, F. Kühnemann, S. Schiller, Appl. Phys. B **80**, 307 (2005)
26 M.M.J.W. van Herpen, S.E. Bisson, F.J.M. Harren, Opt. Lett. **28**, 2497 (2003)
27 F.G.C. Bijnen, J. Reuss, F.J.M. Harren, Rev. Sci. Instrum. **67**, 2914 (1996)
28 D. Halmer, G. von Basum, P. Hering, M. Mürtz, Rev. Sci. Instrum. **75**, 2187 (2004)
29 D.J.M. Stothard, I.D. Lindsay, M.H. Dunn, Opt. Express **12**, 502 (2004)
30 A.V. Smith, *SNLO* software, 4.0 edn. (2005)
31 L.S. Rothman, D. Jacquemart, A. Barbe, D.C. Benner, M. Birk, L.R. Brown, M.R. Carleer, C. Chackerian, K. Chance, L.H. Coudert, V. Dana, V.M. Devi, J.M. Flaud, R.R. Gamache, A. Goldman, J.M. Hartmann, K.W. Jucks, A.G. Maki, J.Y. Mandin, S.T. Massie, J. Orphal, A. Perrin, C.P. Rinsland, M.A.H. Smith, J. Tennyson, R.N. Tolchenov, R.A. Toth, J. Vander Auwera, P. Varanasi, G. Wagner, J. Quantum Spectrosc. Radiat. Transf. **96**, 139 (2005)
32 M.D. Levitt, J.K. Furne, M. Kuskowski, J. Ruddy, Clin. Gastroenterol. Hepatol. **4**, 123 (2006)
33 A. Henderson, R. Stafford, Opt. Express **14**, 767 (2006)